JACS
JOURNAL OF THE AMERICAN CHEMICAL SOCIETY
pubs.acs.org/JACS
Article

Running Wild through Dirhodium Tetracarboxylate-Catalyzed Combined CH(C)-Functionalization/Cope Rearrangement Landscapes: Does Post-Transition-State Dynamic Mismatching Influence Product Distributions?

Wentao Guo and Dean J. Tantillo*

Cite This: J. Am. Chem. Soc. 2024, 146, 7039−7051
Read Online
ACCESS | Metrics & More | Article Recommendations | Supporting Information

ABSTRACT: A special type of C−H functionalization can be achieved through C−H insertion combined with Cope rearrangement (CHCR) in the presence of dirhodium catalysts. This type of reaction was studied using density functional theory and *ab initio* molecular dynamics simulations, the results of which pointed to the dynamic origins of low yields observed in some experiments. These studies not only reveal intimate details of the complex reaction network underpinning CHCR reactions but also further cement the generality of the importance of nonstatistical dynamic effects in controlling Rh_2L_4-promoted reactions.

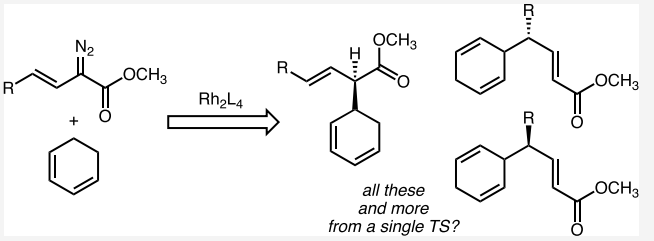

INTRODUCTION

Dirhodium tetracarboxylates (and related carboxylic acid derivatives), Rh_2L_4, have emerged as potent catalysts for various organic reactions due to their high reactivity and selectivity.[1−6] Among these reactions, C−H functionalization[7−9] and cyclopropanation[10−12] have gained significant attention due to their ready integration into synthetic schemes targeting complex molecules. The mechanisms of Rh_2L_4-catalyzed C−H functionalization reactions have been extensively investigated through a combination of experimental and density functional theory (DFT)-based computational studies, which have provided valuable insights into the electronic structure of the key [Rh] carbene intermediate, N_2 extrusion and C−H insertion transition structures (TSs), and the roles of both the metals and ligands of the catalyst in facilitating reaction.[13−20] In general, but not always, H-transfer and C−C bond formation are combined into a concerted process in which these events can occur synchronously or asynchronously. In some cases (the number is growing), post-transition state bifurcations (PTSBs)[21−27] have been found to result in two downhill pathways from an apparent TS for C−H insertion.[28−31] For example, Rh_2L_4-promoted β-lactonization has been shown to involve an ambimodal TS followed by pathways downhill in potential energy that lead to the lactone product or fragmentation products (Scheme 1, left).[28,29] Here, we examine another, seminal, case of a PTSB intruding on a Rh_2L_4-catalyzed C−H insertion reaction (Scheme 1, bottom right),[30,31] along with a related cyclopropanation reaction (Scheme 1, top right), employing modern *ab initio* molecular dynamics (AIMD) simulations to characterize the nonstatistical dynamic effects that control product selectivity. It is perhaps not surprising that we now postulate that PTSBs are common in Rh_2L_4-promoted reactions.

In the realm of Rh_2L_4-catalyzed C−H insertion reactions, the "combined C−H functionalization/Cope rearrangement" (CHCR) reaction discovered by Davies and Lian in 1998 has been extensively studied using various chiral dirhodium catalysts, leading to highly enantio- and diastereoselective versions.[30] Experiments and DFT calculations from Davies and Autschbach and co-workers on these reactions revealed that [Rh] carbene insertion into allylic C−H bonds likely involves a PTSB leading to two products that are related by a Cope rearrangement[30,31] This was the first proposal of a PTSB for a Rh_2L_4-catalyzed reaction, and one that intervenes in a reaction of great synthetic utility. Computations indicated that C−H insertion and C−C bond formation occurred asynchronously with the computed intrinsic reaction coordinate (IRC) leading to the CHCR product (the major product found experimentally); however, the reaction coordinate involved a flat region. Experimental outcomes with some less selective substrates and Rh_2L_4 catalysts are shown in Scheme 2 (many other CHCR reactions are quite selective).[30−33] These results are indeed consistent with the presence of a PTSB, and here

Received: January 9, 2024
Revised: February 8, 2024
Accepted: February 13, 2024
Published: February 28, 2024

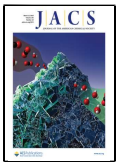

https://doi.org/10.1021/jacs.4c00382
J. Am. Chem. Soc. 2024, 146, 7039−7051

Scheme 1. (a) Illustrated PTSB-Involved C−H Insertion in a Previous Work;[29] (b) C−H and C−C Activation of a C═C π Bond-Containing Substrate Facilitated by [Rh] with Plausible PTSB Dynamic Behavior[a]

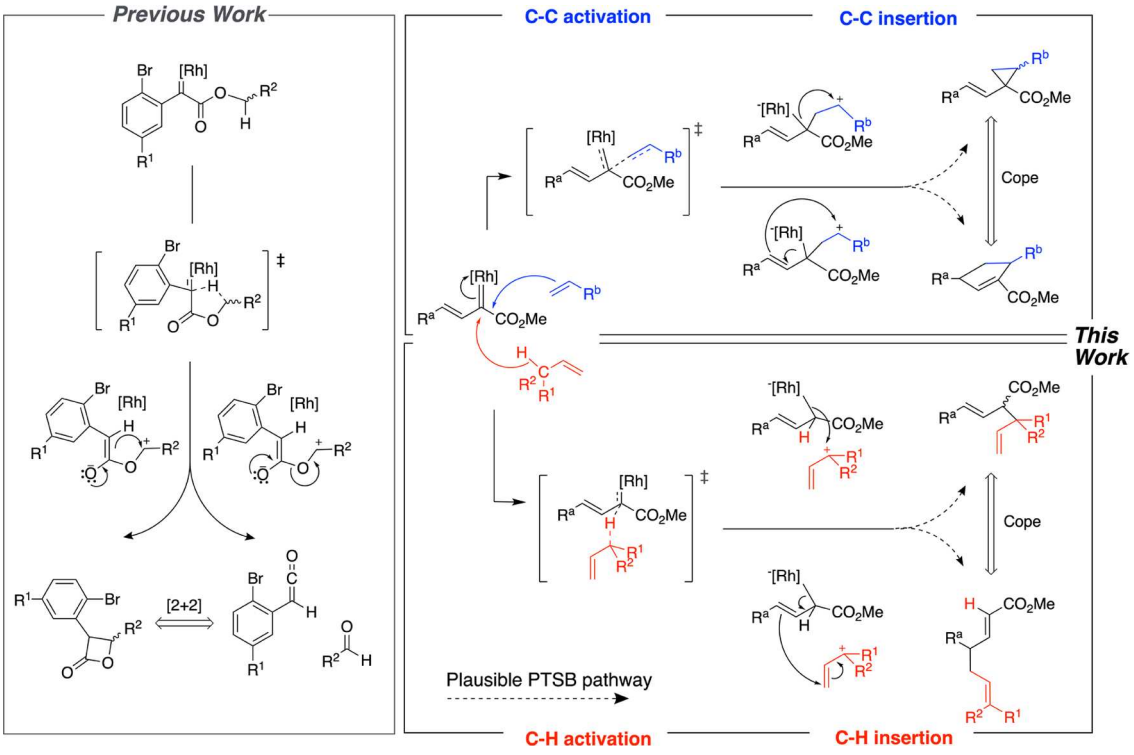

[a][Rh] = Rh_2L_4. Structures with curved arrows are not discrete intermediates but are shown to help readers connect TSs to products.

Scheme 2. Selected Experimental Results[31−33]

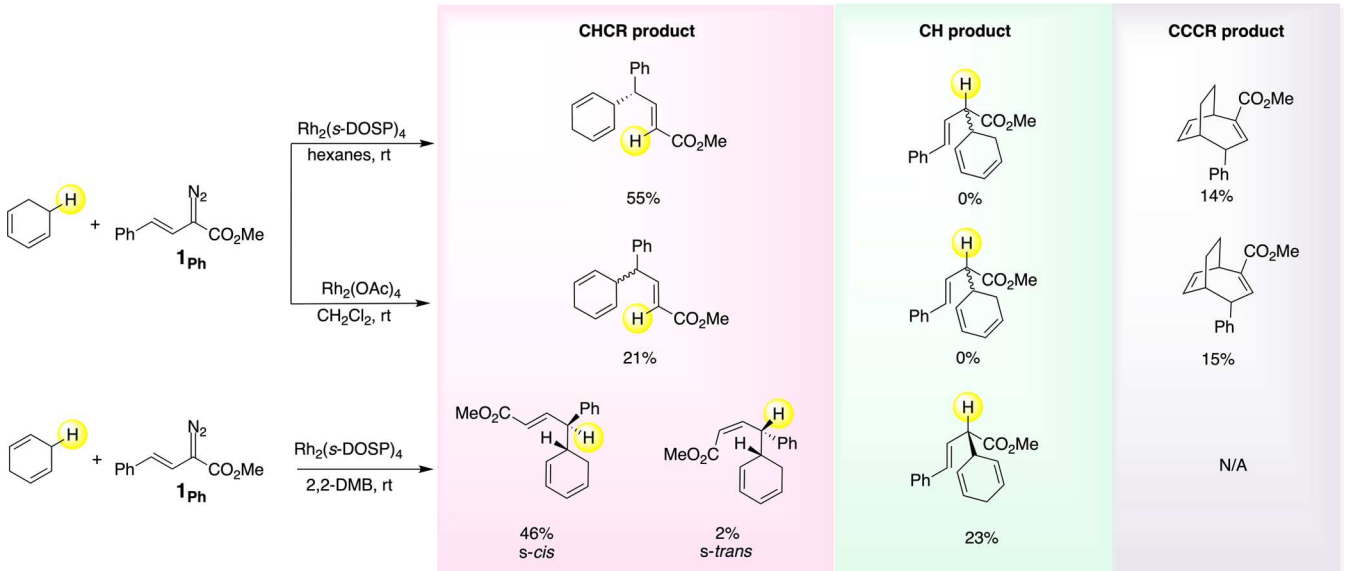

we aim to provide results from AIMD simulations that confirm that both products are directly accessible from the C−H insertion transition state for these reactions and provide insights into the factors controlling selectivity.[34] In addition, the presence of C═C π bonds in the reactants leads to a competition between C−H and C═C functionalization; Scheme 2 shows that products of the C═C functionalization are also sometimes observed. We also explore whether the TS for C−C bond formation is followed by a bifurcation that provides pathways to two C−C functionalized products, one a cyclopropane, that are also related by a Cope rearrangement (Scheme 1, top right), another reaction studied experimentally by Davies and co-workers.[35,36] We refer to this reaction as a "combined C−C functionalization/Cope rearrangement" (CCCR).

These networks of reactions are much more complex than those encountered in our previous AIMD studies on Rh_2L_4-promoted β-lactone formation via C−H insertion.[28,29] As a result, the work described here not only bears on the generality of nonstatistical dynamic effects in Rh_2L_4-promoted reactions

https://doi.org/10.1021/jacs.4c00382
J. Am. Chem. Soc. 2024, 146, 7039−7051

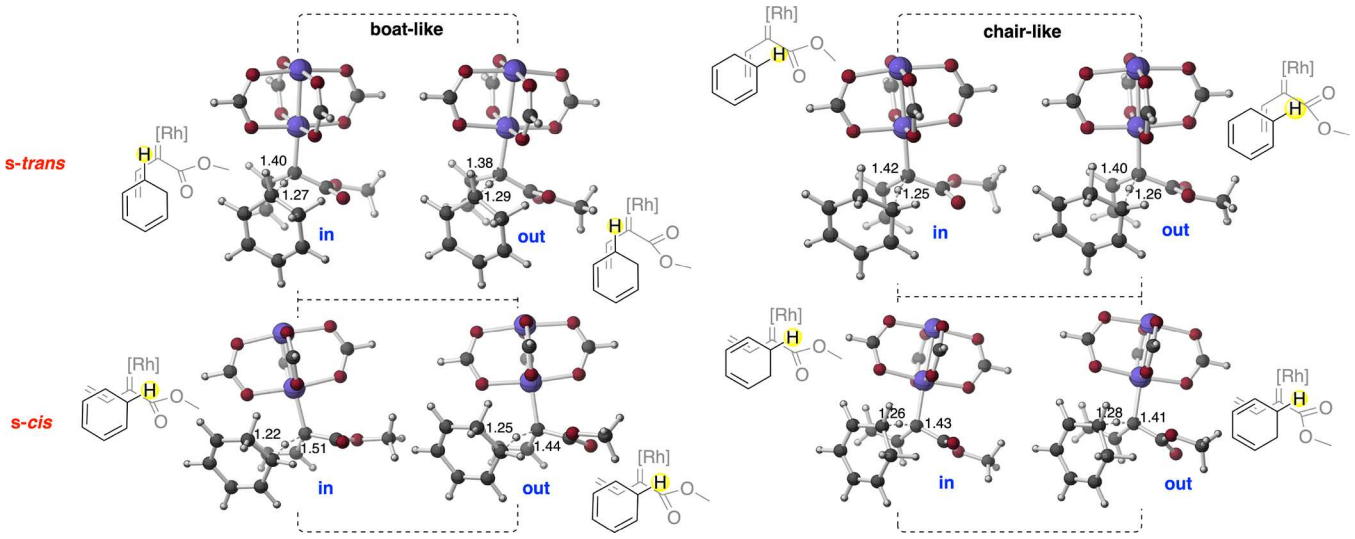

Figure 1. Model system C−H insertion TS conformations with key bond lengths in Å.[59] See the Supporting Information for the geometries of C−C activation TSs.

Table 1. $\Delta G^{\ddagger}$ and IRC Products for the C−H Activation shown in Figure 1[a]

	s-cis				*s-trans*			
	chair		boat		chair		boat	
conformation	in	out	in	out	in	out	in	out
$\Delta G^{\ddagger}$	5.3	5.2	7.5	8.8	5.9	6.4	7.3	7.6
IRC product	CHCR	CHCR	CHCR	CHCR	CHCR	CHCR	elimination	CHCR

[a]Energies are in kcal/mol and are relative to the $G_{1,3\text{-cyclohexadiene}}$ + the best $G_{Rh\text{-carbene}}$ form at the B3LYP-D3(0)/6-311+G(d,p)+LANL2DZ//B3LYP-D3(0)/6-31G(d)+LANL2DZ level of theory (gas phase).

but also tests the limits of our modeling approaches. It also sets the stage for AIMD investigations on the larger systems whose reaction coordinates were previously studied by Davies and co-workers.[31]

COMPUTATIONAL METHODS

Structures. DFT calculations for this study were conducted using *Gaussian16 Rev. C.01* using B3LYP-D3(0) and a mixed basis set consisting of 6-31G(d) for C, H, and O and LANL2DZ for Rh.[37−42] Single-point energy calculations were carried out on optimized structures using B3LYP-D3(0)/6-311+G(d,p)+LANL2DZ and M06/6-311+G(d,p)+LANL2DZ levels of theory (see the Supporting Information for details).[43,44] These functional/basis set combinations have been used successfully in previous studies of similar reactions.[28,29,45] For example, in our previous work, we confirmed that the relatively inexpensive B3LYP-D3(0)/6-31G(d)+LANL2DZ is suitable for such reactions through a benchmarking study with various levels of theory.[29] In simulations involving solvent, the DCM environment was represented using the polarizable continuum model (PCM) for both DFT calculations and AIMD simulations.[46,47] Triplet states were ignored due to their significantly higher energies than singlets. TSs were identified by the presence of only one imaginary vibrational frequency, and their connection to minima was confirmed through IRC analysis (see Supporting Information for plots).[48−50] Coordinates for all computed structures are available at https://iochem-bd.bsc.es/browse/handle/100/315418[51]

Dynamics. AIMD simulations were run using Singleton's *Progdyn* package in the NVE ensemble at room temperature (298.15 K) with a time step of 1 fs.[52] Trajectories were propagated using the Verlet algorithm. Selectivity was determined by comparing the number of trajectories that connect the [Rh] carbene to each product minimum. To minimize recrossing, variational transition states, located using the RODS method in *Polyrate/Gaussrate*, were used to initiate downhill AIMD trajectories.[53−55] We performed three types of dynamic simulations: quasi-classical downhill, classical downhill, and uphill.[56,57] Quasi-classical simulations involved providing a zero-point energy (ZPE) for each vibrational mode. However, since the time required to form a product in some systems exceeded 1 ps (1000 steps), causing us to worry about ZPE leakage effects,[58] we also carried out classical downhill simulations. We also attempted to initiate uphill dynamics from [Rh] carbenes by stretching the C−H bond that would break in the insertion reaction, but this approach was unsuccessful (see the Supporting Information for details).

RESULTS AND DISCUSSION

Parent System. We first discuss a simplified reaction involving methyl 2-methylenebut-3-enoate bound to $Rh_2(HCO_2)_4$ and cyclohexadiene as a substrate in the gas phase. This same reaction was previously modeled by Davies and co-workers, where four different conformations of C−H insertion TSs were reported.[31] We located eight different conformations for C−H insertion TSs, however (Figure 1). In addition to the *s-cis*/*s-trans* (referring to the Rh−C−C═C dihedral angle) and chair-like/boat-like (referring to the six atoms involved in the Cope rearrangement) geometries discussed previously,[31] we observed that the orientation of the carbonyl oxygen of the seemingly innocuous ester (in/out labels indicate whether oxygen is inside or outside the gap between 1,3-cyclohexadiene and the [Rh] carbene) also played a critical role in determining product selectivity. C−H insertion TSs with cyclohexadiene in other orientations were explored, but these were higher in energy (see Supporting Information).

Selectivity, or Not. The data in Table 1 indicate that chair-like C−H insertion transition states are lower in free energy

https://doi.org/10.1021/jacs.4c00382
J. Am. Chem. Soc. 2024, 146, 7039−7051

Scheme 3. Energy Profile for the Parent System C−H and C−C Activation with Key TSs[a]

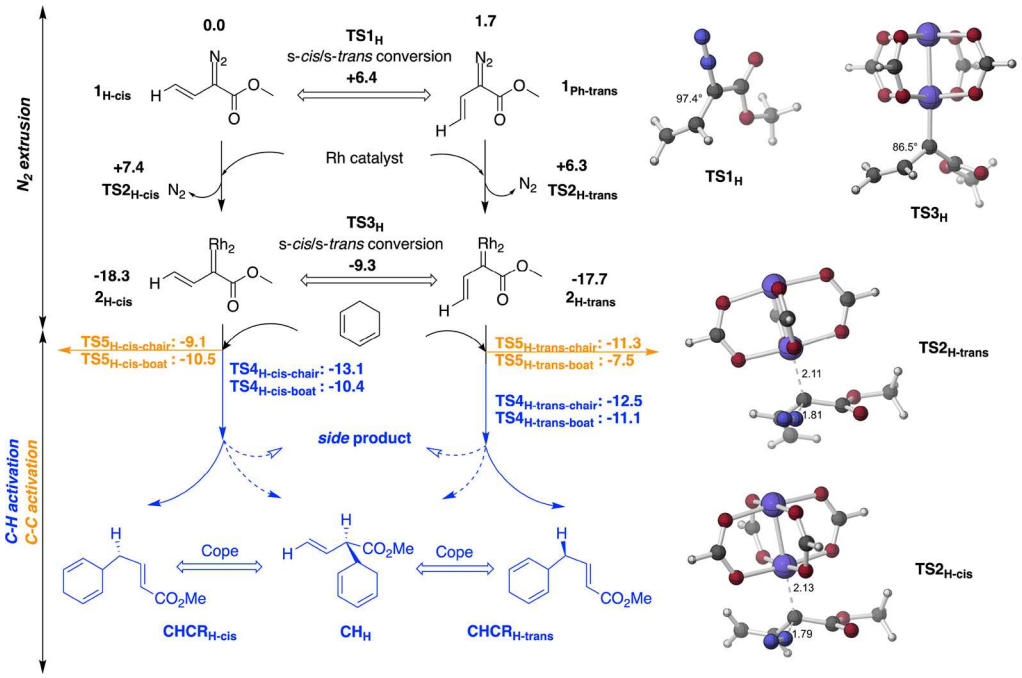

[a]Relative free energies were computed at the B3LYP-D3(0)/6-311+G(d,p)+LANL2DZ//B3LYP-D3(0)/6-31G(d)+LANL2DZ level of theory (gas phase). As the in and out conformations have very similar energies, only the energy of the lower energy one is presented. Selected distances on TSs are shown in Å.[59] Dihedral angles for s-*cis*/s-*trans* conversion TSs are labeled as well. For more information on formation of CCCR products (orange), see the Supporting Information.

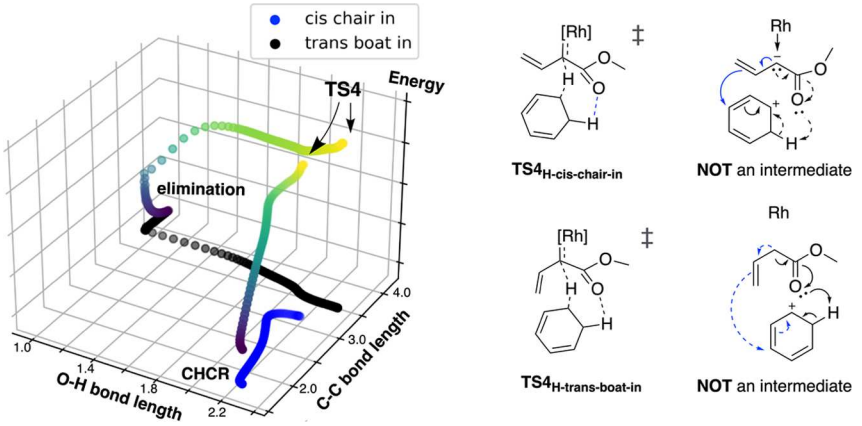

Figure 2. IRCs and their projections of the **TS4**$_{\text{H-cis-chair-in}}$ and the **TS4**$_{\text{H-trans-boat-in}}$ boat-like TSSs on the direction of the product side color by the energy. The C−C bond and the O−H bond formation correspond to the CHCR and elimination of cyclohexadiene, respectively. Critical bonds and arrows are colored by the corresponding products: black—elimination; blue—CHCR.

than boat-like transition states, consistent with previous results.[31] However, since all barriers for C−H insertion are low, we suspected that s-*cis* versus s-*trans* selectivity might be determined prior to C−H insertion, i.e., barriers for interconversion of s-*cis* and s-*trans* species might be higher than those for reaction. The possibilities are outlined in Scheme 3, which also shows computed energetics. The process of switching from s-*cis* to s-*trans* at the [Rh] carbene stage involves a barrier of approximately 9 kcal/mol, which is indeed greater than the barriers computed for C−H activation (Table 1).[31] Consequently, formation of the carbene from the diazo precursor is not inconsequential with regard to selectivity. The s-*cis* and s-*trans* diazo compounds are predicted to differ in energy by 1.7 kcal/mol. Their interconversion is associated with TS (**TS1**$_{\text{H}}$) whose energy is comparable to that of the TSs for N_2 extrusion (**TS2**$_{\text{H-cis}}$ and **TS2**$_{\text{H-trans}}$). N_2 extrusion is also predicted to be very exergonic and releases a gas and so is expected to be irreversible. While all of these considerations complicate matters, considering the accuracy and expected error bars associated with DFT methods of the type used, it is most prudent to predict that little, if any, selectivity is expected. We point out these issues, however, because such a copout may not be possible for other systems.

Reaction Coordinates. As shown in Table 1, an elimination product (benzene) was unexpectedly observed when running an IRC from the *trans*-boat-in C−H insertion TS (**TS4**$_{\text{H-trans-boat-in}}$ in Figure 2). The formation of the elimination product involves the shift of a proton from the sp^3

https://doi.org/10.1021/jacs.4c00382
J. Am. Chem. Soc. 2024, 146, 7039−7051

Scheme 4. (a) Products Found in AIMD Simulations, Arrow Pushing Mechanisms for Each from the "NOT an Intermediate" Ion Pair (to Distinguish CHCR, CH*, and CH Products, Atoms Are Numbered), [Rh] = $Rh_2(HCO_2)_4$; (b) Product Distributions from AIMD Simulations

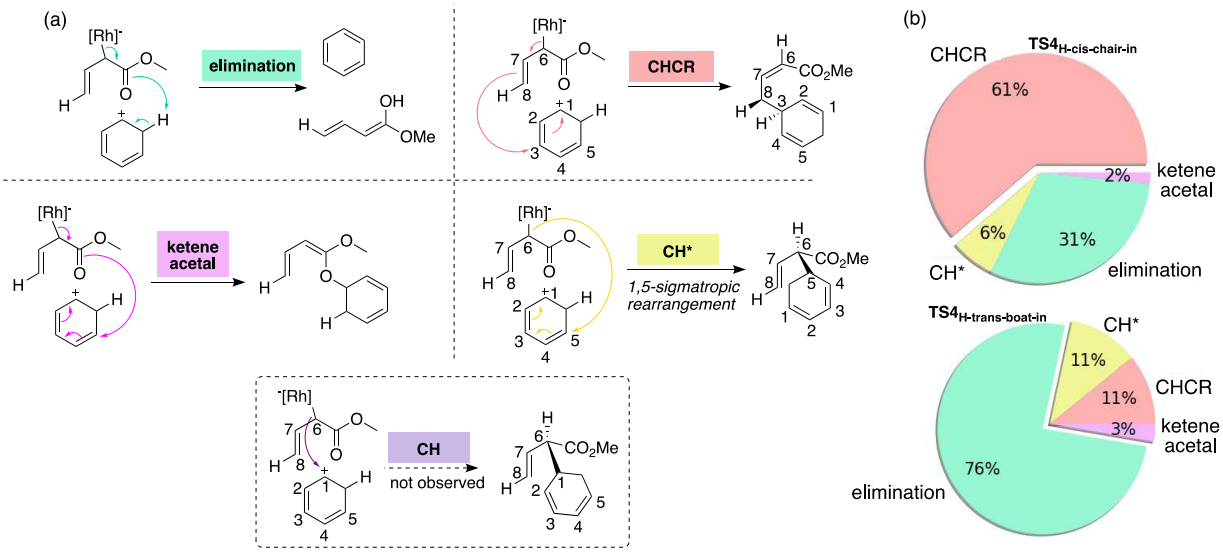

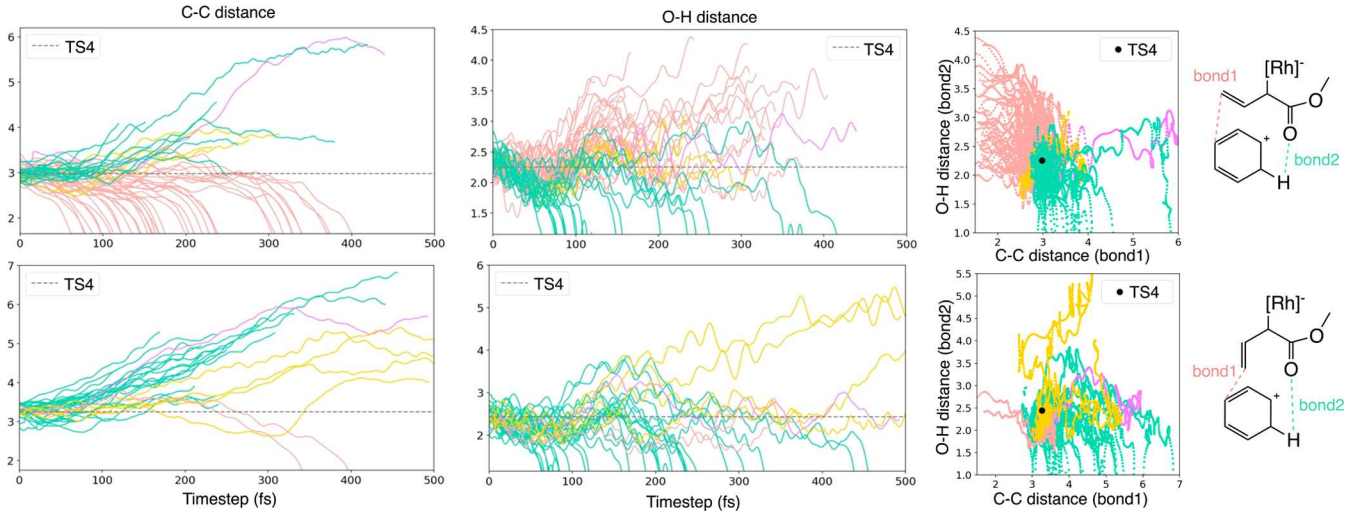

Figure 3. Plots of trajectories from $\mathbf{TS4}_{\text{H-cis-chair-in}}$ (top) and $\mathbf{TS4}_{\text{H-trans-boat-in}}$ (bottom) in terms of the C−C (CHCR product) and O−H (elimination product) distance. (a) C−C distance versus time. (b) O−H distance versus time. (c) 2D projections of trajectories. Color represents the product of corresponding trajectories: **CHCR** in pink, **elimination** in mint, **ketene acetal** in magenta, and **CH*** in yellow.

carbon of the cyclohexadiene not involved in C−H insertion to the nearby oxygen of CO_2Me (in addition to the shift of the hydride from the other sp^3 carbon to the carbene carbon). Thus, the geometry of this TS must have a short H···O distance to access the elimination channel. Among the eight possible conformers, only $\mathbf{TS4}_{\text{H-cis-chair-in}}$ and $\mathbf{TS4}_{\text{H-trans-boat-in}}$ satisfy this requirement, yet their IRCs lead to different products. Is a PTSB involved? To help answer this question, we plotted the two IRCs together in Figure 2, with respect to the distances for the O−H and C−C bonds that would form in elimination and CHCR products, respectively. Both the O−H and C−C bonds are shorter in the geometry of $\mathbf{TS4}_{\text{H-cis-chair-in}}$ (whose IRC leads to the CHCR product) than in $\mathbf{TS4}_{\text{H-trans-boat-in}}$, its IRC showing that the O and H initially approach each other but then move apart as the C−C bond forms through a pathway that descends steeply in energy. In contrast, O and H move toward each other throughout the IRC for $\mathbf{TS4}_{\text{H-trans-boat-in}}$, which describes a longer region of relatively constant energy. In both cases, flat regions of potential energy are observed, which correspond to structures labeled as "NOT an intermediate" in Figure 2, although whether or not such structures have significant lifetimes and can be characterized as entropic intermediates remains to be seen.[60−62] The presence of a "shoulder" on the IRC is a common feature for TSs **TS4**, even when their geometries are not conducive to the formation of an elimination product (see the Supporting Information for the IRC plots), but does this feature suggest that multiple products are accessible from each **TS4**? Answering this question requires AIMD simulations.

Dynamical Tendencies. AIMD simulations were carried out, starting from both $\mathbf{TS4}_{\text{H-cis-chair-in}}$ and $\mathbf{TS4}_{\text{H-trans-boat-in}}$, revealing several dynamic behaviors: (1) For both TSs, four different product minima were found to be linked to the [Rh] carbene (Scheme 4): the **CHCR** product, the **elimination** product, a **CH*** product (the same molecular structure as the direct C−H insertion product but resulting from a formal 1,6-

https://doi.org/10.1021/jacs.4c00382
J. Am. Chem. Soc. 2024, 146, 7039−7051

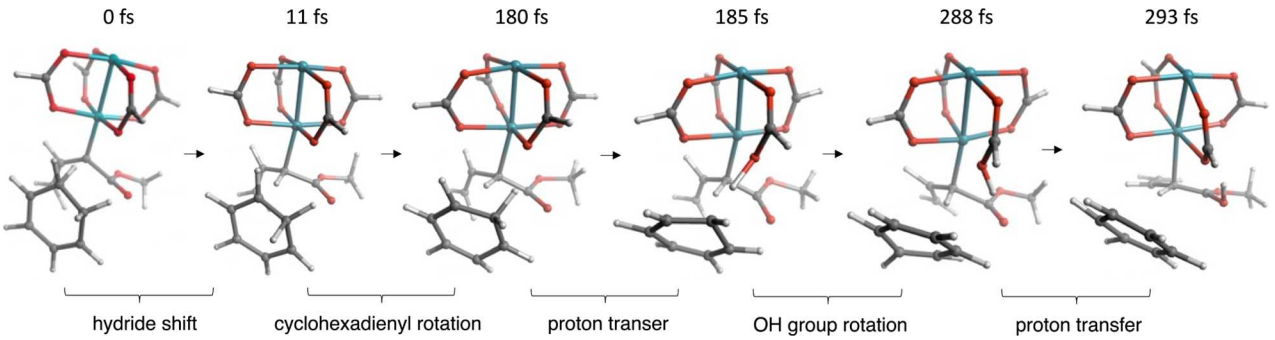

Figure 4. Snapshots taken from a trajectory in which an HCO_2 ligand facilitates elimination for $\mathbf{TS4}_{\text{H-trans-boat-in}}$.

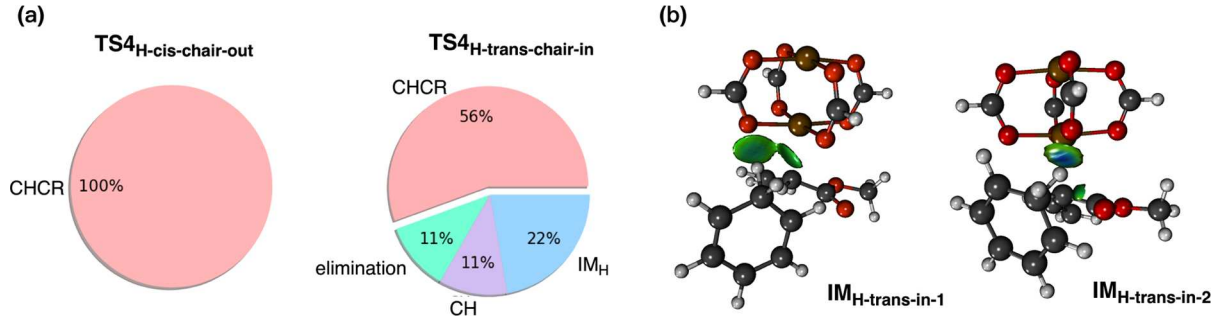

Figure 5. (a) Product distribution from AIMD simulations for $\mathbf{TS4}_{\text{H-cis-chair-out}}$ and $\mathbf{TS4}_{\text{H-trans-chair-in}}$. (b) IGMH graph for two $\mathbf{IM}_{\text{H}}$ minima (isovalue = 0.005) depicted by *Multiwfn* and *VMD*.[64,65] The hydrogen bonds in $\mathbf{IM}_{\text{H-trans-in-1}}$ are between two HCO_2 groups and the acidic H, while in **IMH-trans-in-2**, one hydrogen bond involves the carbanion ester.

sigmatropic rearrangement step following hydride transfer), and a **ketene acetal** product. As shown in Scheme 4, all four products can be rationalized as arising from the "NOT an intermediate" ion pair associated with the shoulder region of the IRCs discussed above, consistent with this region of the potential energy surface being flat and having multiple exit channels. (2) The dynamically preferred products are the IRC products (Table 1 and pie charts in Scheme 4). (3) None of the trajectories lead directly to the C−H insertion product or even show a tendency to do so (details in the Supporting Information). (4) The time necessary for product formation shows substantial variability for both TSs (Figure 3), again consistent with a flat energy surface or an entropic intermediate. For example, the time required for the formation of an elimination product from $\mathbf{TS4}_{\text{H-trans-boat-in}}$ ranges from 60 to 450 fs. (5) The ion pair generally explores a broad region close to each TS before settling into a minimum, as revealed by the 2D trajectory projections in Figure 3 (right). This observation is consistent with the fact that the key O−H and C−C bonds are not directly involved in the hydride shift, minimizing the likelihood of a ballistic (momentum) effect (additional details can be found in the Supporting Information).[63] While the lack of a ballistic effect implies that the initial momentum of the system does not have a direct impact on the dynamic effects, it may still affect the behavior of the nonstatistical intermediate to some extent. (6) Two special cases were observed in which proton migration was assisted by HCO_2 ligands during elimination from $\mathbf{TS4}_{\text{H-trans-boat-in}}$. Four consecutive stages were observed in these cases (e.g., Figure 4): hydride shift (fast, 0−11 fs), counterclockwise rotation of the protonated benzene (slow, 11−180 fs), deprotonation by HCO_2 (fast, 180−185 fs), OH group reorientation (slow, 185−288 fs), and proton shuttling to the ester carbonyl O (fast, 288−293 fs). These trajectories suggest that even in the absence of an appropriate initial elimination pose, there is still a possibility that the proton is captured by a carboxylate before any C−C bond is formed.

To investigate the general importance of the putative ion pair entropic intermediate ($\mathbf{IM}_{\text{H}}$), we also examined $\mathbf{TS4}_{\text{H-cis-chair-out}}$ and $\mathbf{TS4}_{\text{H-trans-chair-in}}$ with AIMD simulations. The acidic proton in the former is far from both the catalyst and the ester group, while the acidic proton in the latter is located away from the ester group but between two HCO_2 ligands. These two TSs also have low relative energies (Table 1). The AIMD simulations for $\mathbf{TS4}_{\text{H-cis-chair-out}}$ produced only the CHCR product, whereas those for $\mathbf{TS4}_{\text{H-trans-chair-in}}$ led to four different products (Figure 5, left). The four products included two new products, a product of direct C−H insertion (**CH**) and $\mathbf{IM}_{\text{H}}$ as an end point; **CH*** and **ketene acetal** products were not observed. Here, $\mathbf{IM}_{\text{H}}$ was confirmed to be a minimum on the potential energy surface by optimizing the end points of the $\mathbf{IM}_{\text{H}}$-forming trajectories. We hypothesize that the emergence of this shallow intermediate (which will be converted to product structures at longer times) is due to two CH···O hydrogen bonds between CH protons on the cyclohexadienyl cation substructure and oxygens of HCO_2 groups on the catalyst and/or the ester (Figure 5, right). Additionally, the perpendicular pose of the carbanion and protonated benzene makes it inaccessible to either the C−H insertion or the CHCR exit channels.

Although the trajectories show considerable variability, there is one common trait observed among all of them: regardless of their initial geometry, the terminal alkene rotates clockwise after the hydride shift. To understand why, we examined the vibrations corresponding to the imaginary frequencies of the TSs. These are visualized for two TSs in Figure 6. These vibrations lead to the terminal alkene rotating away from the hexadiene into a mutually perpendicular orientation that

https://doi.org/10.1021/jacs.4c00382
J. Am. Chem. Soc. 2024, 146, 7039−7051

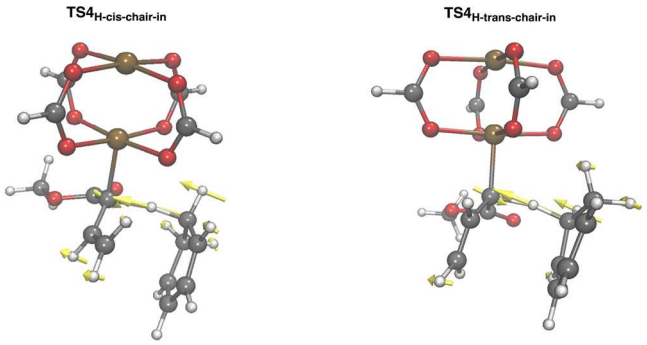

Figure 6. Vector representation of the imaginary vibrational mode, visualized by VMD.[65]

impedes the formation of both CHCR and direct C−H insertion products. In contrast to dynamic matching,[25,56,61,66−69] where the momentum possessed by a molecule as it falls down the energy hill after passing the transition state is used to enhance formation of a subsequent product; here, that momentum actively drives trajectories away from products, allowing the ion pair structure to persist. We propose the term "dynamic mismatching" for such an effect, i.e., when post-TS momentum drives a trajectory away from the product of an IRC rather than toward it. Note that this effect is distinct from the increase in "flexibility" that leads to entropic intermediates. This effect is more detrimental to the s-*trans* TSs, as their terminal carbons are moving quickly away from the cyclohexadiene. Consequently, more time is required for the cyclohexadienyl cation to become appropriately aligned to form the CHCR product. Indeed, for $\mathbf{TS4}_{\text{H-trans-chair-in}}$, CHCR product-forming trajectories are on average (397 fs) longer than those for $\mathbf{TS4}_{\text{H-cis-chair-in}}$ (214 fs).

Putting It All Together. The results of our AIMD simulations make it clear that the reactivity of this system is far more complex than that of combined C−H insertion and Cope rearrangement. Based on our AIMD results, we sought out additional PES minima and have identified a total of six that can be reached from the C−H activation TS (Scheme 5): direct C−H insertion (**CH**), Cope rearrangement combined with CH insertion (**CHCR**), formal [1,6]-sigmatropic rearrangement combined with C−H insertion (**CH***), ion pair intermediate ($\mathbf{IM}_{\mathbf{H}}$), C−O bond formation (**ketene acetal**), and elimination (**benzene**) products. Note that we do not consider this scenario to reflect a "post-transition-state hexafurcation"; rather, it reflects an energy surface with flat regions having multiple exit channels, consistent with the early calculations on reaction coordinates from Davies et al. (see the Supporting Information for details on AIMD simulations initiated with other stationary points and IRCs, which often have "shoulders").[31] Given the complex nature of the potential energy surfaces involved, it is challenging (and we would argue, not so useful) to capture all stationary points in a classic two-dimensional energy profile (energy versus structure). Instead, we summarize the connectivity between minima and TSs in Scheme 5 through the use of various types of arrows: double-headed arrows (not resonance arrows!) link the minima for which we have identified a TS for their interconversion, whereas conventional single-headed arrows indicate structures connected to **TS4** by AIMD trajectories alone (see the Supporting Information for an alternative dimensionality-reducing approach based on principal component analysis). The top of Scheme 5 shows the s-*trans*-chair-in system, for which we were able to locate two $\mathbf{IM}_{\text{H-trans}}$ minima and eight TSs that connect products. The two geometries of $\mathbf{IM}_{\text{H-trans}}$ originate from either a clockwise or counterclockwise rotation following the initial hydride shift event. To indicate how this rotation impacts branching in dynamics simulations, the arrows surrounding the $\mathbf{post\text{-}TS4}_{\text{trans-chair-in}}$ structure are drawn clockwise or counterclockwise based on the sense of rotation in trajectories that lead to the products at the end of those arrows. While the **CH*** product could potentially be achieved via a clockwise reaction pathway, we did not observe any trajectories leading to its formation in this system. Initially, we discovered that $\mathbf{IM}_{\text{H-trans-in-2}}$ is linked to two types of elimination processes (where the proton is transferred to either the ester group or the HCO_2 ligand) and the **ketene acetal** via $\mathbf{TS6}_{\text{H-trans}}$, $\mathbf{TS7}_{\text{H-trans}}$, and $\mathbf{TS8}_{\text{H-trans}}$. While $\mathbf{TS7}_{\text{H-trans}}$ is higher in potential energy than $\mathbf{IM}_{\text{H-trans-in-2}}$, it is actually slightly lower in free energy than $\mathbf{IM}_{\text{H-trans-in-2}}$. A similar reaction network is observed for the s-*cis*-chair-in system (Scheme 5, bottom), although it is slightly simpler. For example, only one $\mathbf{IM}_{\text{H-cis-chair-in}}$ minimum was found, but no trajectories were trapped in this structure.

Phenyl Substitution. Replacing one terminal hydrogen of the simple system described above with a phenyl group and HCO_2 ligands with OAc ligands leads to a system that was reported by Davies in 2007 (Scheme 2, center).[33] For reactant $\mathbf{1}_{\text{Ph}}$ (Schemes 2 and 6), a 1.4:1 ratio of CHCR:CCCR products with a combined yield of 36% was observed. To determine whether the relatively low yield (21%) of CHCR products might be the result of dynamic mismatching, comprehensive DFT calculations on the potential energy surface for this system and AIMD simulations were carried out (here with the PCM solvation model).

Adding a phenyl group to the substrate alkene leads to a more challenging interconversion between s-*cis* and s-*trans* [Rh] carbene $\mathbf{2}_{\text{Ph}}$, which now is predicted to have a free energy barrier (via $\mathbf{TS3}_{\text{Ph}}$) of approximately 16 kcal/mol (Scheme 6). In contrast, the predicted barrier for the s-*cis*/s-*trans* interconversion of $\mathbf{1}_{\text{Ph}}$ remains low. This difference is likely a result of steric clashes with the ligands on the catalyst that restrict rotation of the styrenyl group. Since the barrier for interconversion of the [Rh] carbenes is higher than those for conversion to products, selectivity should come from the N_2 extrusion process, for which no significant preference for s-*cis* versus s-*trans* $\mathbf{TS2}_{\text{Ph}}$ is predicted. Thus, we expect both the *cis* and *trans* low-energy chair-like **TS4**s to contribute essentially equally when predicting product distributions from AIMD simulations.

A challenge with running quasi-classical AIMD simulations for this system was that approximately 10% of all trajectories did not form products within 1000 fs. This may reflect the presence of an entropic intermediate differing from $\mathbf{IM}_{\text{Ph}}$, but given the risk of ZPE leakage, we also carried out classical downhill AIMD simulations. The outcomes of both quasi-classical (with trajectories that did not form products not included) and classical AIMD simulations are presented in Figure 7. In the classical simulations, all trajectories managed to terminate within 1000 fs. This, in turn, boosted the proportion of trajectories forming the CHCR product, seemingly since the kinetic energy of the system is not sufficiently large and distributed appropriately for the molecule to explore around the $\mathbf{IM}_{\text{trans-Ph}}$ region but instead remains localized around the minimum energy path leading to the CHCR product. For s-*trans* $\mathbf{TS4}_{\text{Ph-trans-chair-in}}$, the product

https://doi.org/10.1021/jacs.4c00382
J. Am. Chem. Soc. 2024, 146, 7039−7051

Scheme 5. Reaction Networks for s-*trans*-Chair-in and s-*cis*-Chair-in Systems[a]

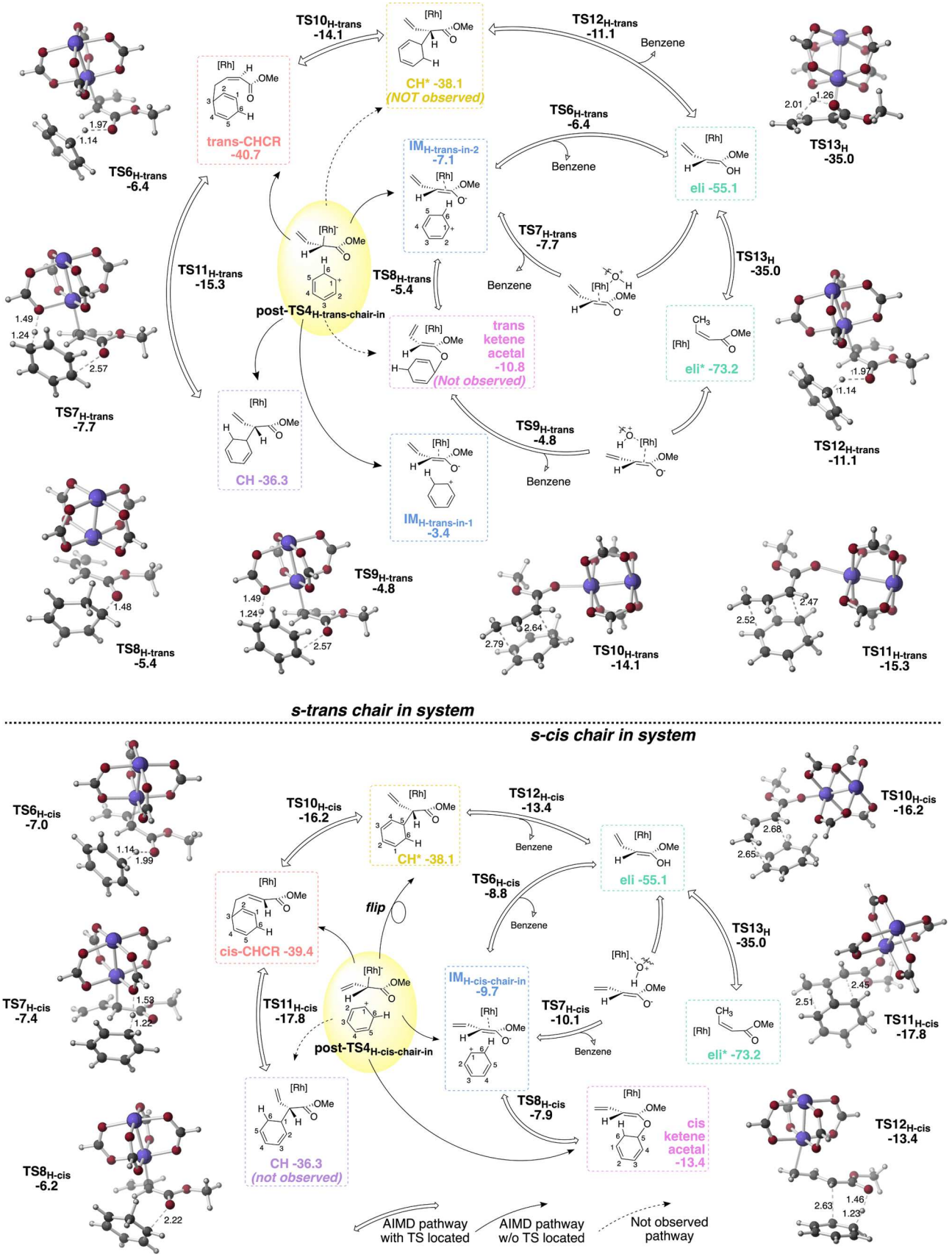

[a]Free energies relative to the best [Rh] carbene/1,3-cyclohexadiene complex are shown (kcal/mol).

https://doi.org/10.1021/jacs.4c00382
J. Am. Chem. Soc. 2024, 146, 7039−7051

Scheme 6. Energy Profile for the Phenyl-Substituted System[a]

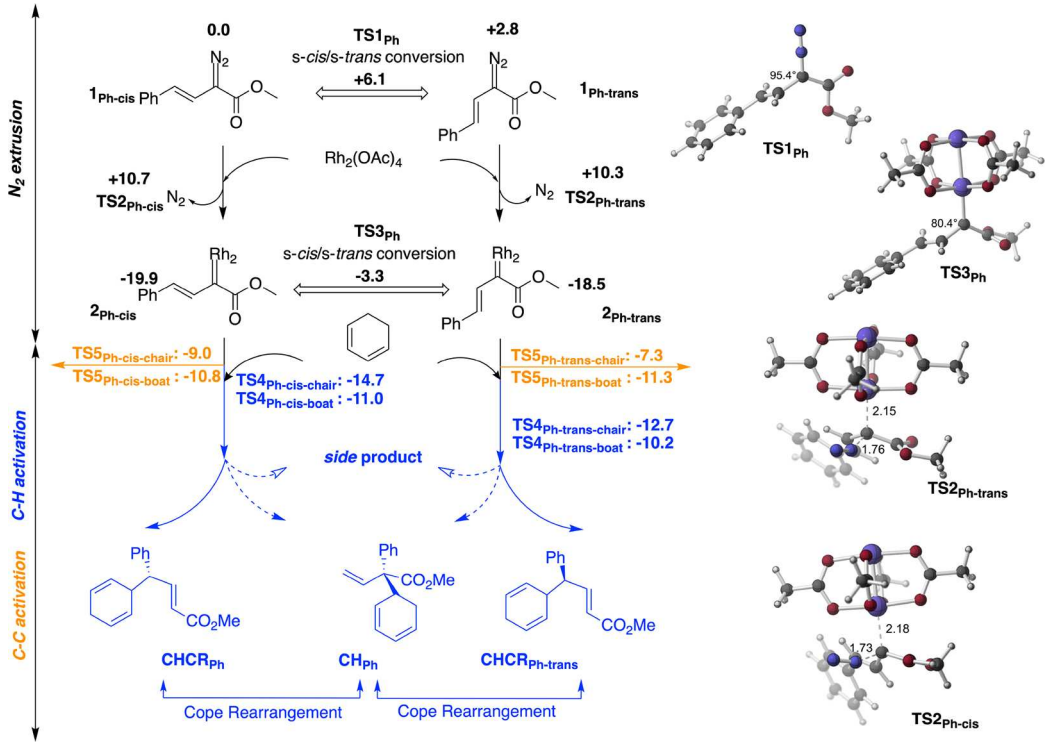

[a]Relative free energies were computed at the PCM(DCM)-B3LYP-D3(0)/6-311+G(d,p)+LANL2DZ//PCM(DCM)-B3LYP-D3(0)/6-31G-(d)+LANL2DZ level of theory. As the in and out conformations have very similar energies, only the energy of the lower energy one is presented. Selected distances on TSs are shown in Å.[59] For more information on formation of CCCR products (orange), see the Supporting Information.

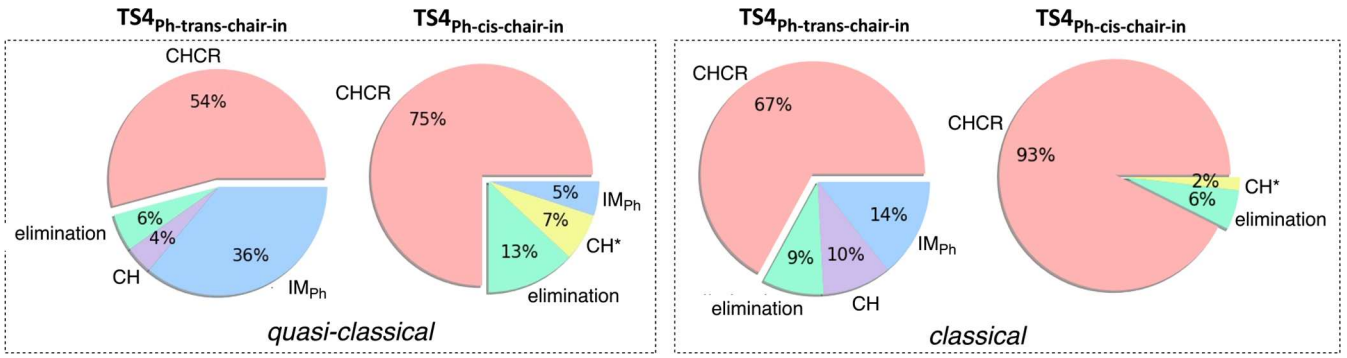

Figure 7. Results of AIMD simulations initiated from $\mathbf{TS4_{Ph\text{-}trans\text{-}chair\text{-}in}}$ and $\mathbf{TS4_{Ph\text{-}cis\text{-}chair\text{-}in}}$. $\mathbf{IM_{Ph}}$ is analogous to $\mathbf{IM_H}$, containing a phenyl group for R instead of H.

distribution from quasi-classical AIMD simulations is similar to that of the model system (Figure 5), but again, removing ZPE increases CHCR product formation. Overall, combining the results from the s-*trans* and s-*cis* systems, more CHCR products are expected for the phenyl-substituted system but the nature of the potential energy surface and associated dynamic behavior is expected to lead to very little C−H insertion product (none was observed experimentally) and a nontrivial amount of side products (consistent with the experimentally reported low yield). Compared to the model system, the mismatching effect may be alleviated due to the increased difficulty in rotating the larger styrenyl group. Note also that TSs leading to CCCR products (**TS5**) may be close enough in free energy to compete as well (Scheme 6; see the Supporting Information for dynamics results).

A Larger Catalyst. In contrast to the $Rh_2(OAc)_4$-catalyzed reaction just described, Davies and co-workers observed a good yield (55%) of the CHCR product when using $Rh_2(s\text{-DOSP})_4$ as a catalyst (Scheme 2, top).[32] Again, simple C−H insertion product was not reported. To characterize the role of $Rh_2(s\text{-DOSP})_4$, we employed a model that truncates the long alkyl chains of the ligands (Figure 8a). The selectivity obtained with $Rh_2(s\text{-DOSP})_4$ was previously proposed to originate from a favored $\alpha\beta\alpha\beta$ ligand arrangement, common for Rh_2L_4 catalysts with bulky ligands.[70,71] However, unlike other common ligands that are fairly rigid, such as TCPTTL, the pyrrolidine and benzenesulfonyl groups of DOSP have considerable rotational flexibility.[6,29,72] Thus, it is perhaps not surprising that our conformational searches on $Rh_2(s\text{-DOSP})_4$ led to no ligand orientations that can be described simply as either pointing upward or downward with respect to the Rh−Rh unit. We

https://doi.org/10.1021/jacs.4c00382
J. Am. Chem. Soc. 2024, 146, 7039−7051

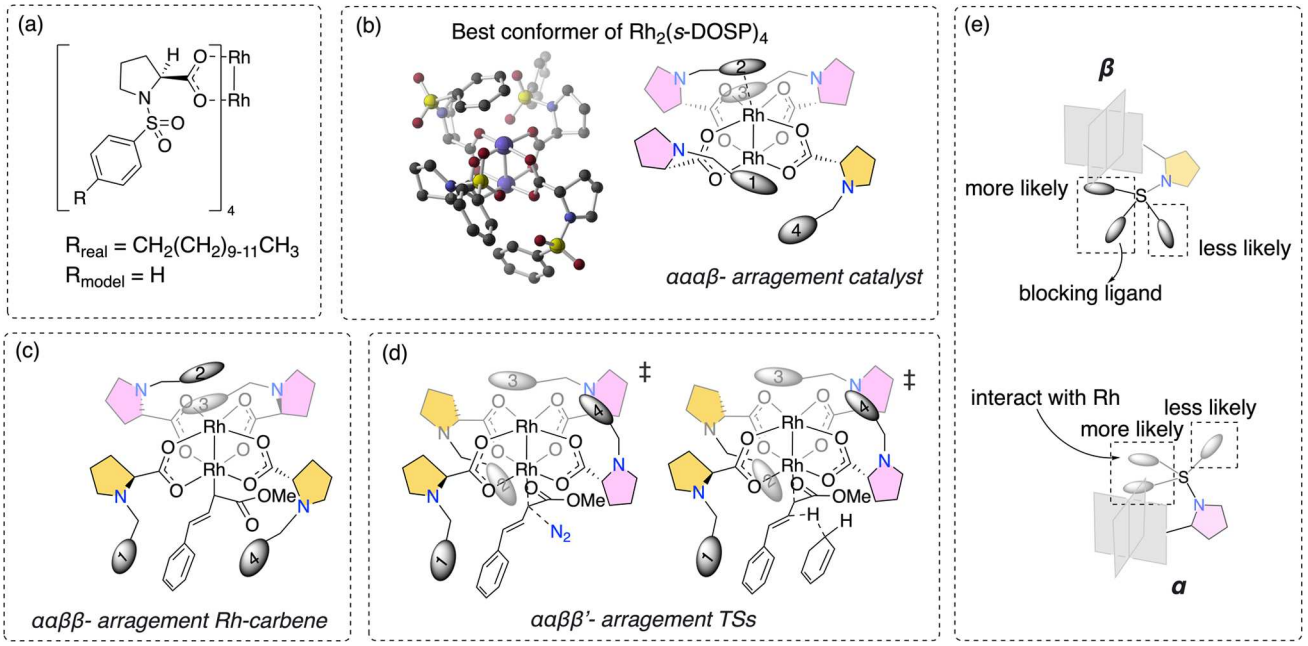

Figure 8. (a) Rh_2(*s*-DOSP)$_4$ simplification used for calculations. (b) The lowest-energy Rh_2(*s*-DOSP)$_4$ geometry and schematic illustration of the lowest-energy Rh-carbene geometry. (c) Schematic illustration of the lowest-energy Rh-carbene geometry. (d) Schematic illustration of the lowest-energy N_2 extrusion and C−H activation TS geometry. (e) Schematic illustration of the plausible conformations of Rh_2(*s*-DOSP)$_4$ and its flexible ligands.

explored the geometrical space of Rh_2(*s*-DOSP)$_4$, the [Rh] carbene, and the N_2 extrusion TS using *xTB-CREST* (see the Supporting Information for details).[73] The lowest energy conformer of Rh_2(*s*-DOSP)$_4$ found has an asymmetrical geometry that we tentatively refer to as *ααaβ* (Figure 8b; see the Supporting Information for other conformers). In the absence of a bound carbene, one benzene ring tends to interact with Rh, but the ligands alter their arrangement to accommodate the substrate, maximizing weak interactions while minimizing steric hindrance with an *ααββ* geometry (e.g., Figure 8c). Another *ααββ* geometry (also called as *ααββ'*) is preferred for the N_2 extrusion TS structure, with one side of the substrate shielded and the other side left open (Figure 8d). Additionally, the shielding ligand promotes an out conformation of the [Rh] carbene, wherein the carbonyl oxygen is oriented toward the shielded direction. A similar geometry is expected for the C−H functionalization TSs as cyclohexadiene approaches (Figure 8d). Moreover, the steric confinement provided by the DOSP ligands may serve to discourage mismatching (due to rotation) for both the s-*cis* and *s*-trans conformations. In short, the DOSP ligands provide a constrictive but malleable binding site.

While AIMD simulations on this system are beyond the scope of this study due to the size and, significantly, flexibility of Rh_2(*s*-DOSP)$_4$, we can propose a hypothesis on the origins of increased selectivity for this system based on the geometries and energies of key structures. While no strong preference was predicted for the s-*trans* or s-*cis* carbene with $Rh_2(OAc)_4$ (Scheme 6), the s-*cis* [Rh] carbene is predicted to be 6 kcal/mol lower in energy than the s-*trans* [Rh] carbene with Rh_2(*s*-DOSP)$_4$ as a result of selective noncovalent interactions with the ligands, and these same interactions are likely to hinder s-*cis*/s-*trans* interconversion. This strong preference for s-*cis* binding with Rh_2(*s*-DOSP)$_4$ is also reflected in the energies of the N_2 extrusion TSs, where s-*cis* dominates with a 4 kcal/mol energy barrier. Even though both s-*cis* and s-*trans* carbenes lead to CHCR products, we have shown above that the s-*cis* conformation results in a higher selectivity for formation of CHCR products over side products in AIMD simulations, for both the simple model system and the phenyl-substituted system with $Rh_2(OAc)_4$. If this dynamic preference persists with Rh_2(*s*-DOSP)$_4$, the bias induced by the ligand for the s-*cis* conformation may well be the indirect source of enhanced CHCR product formation.

CONCLUSIONS

The results of our quantum chemical calculations, both static and dynamic—which add to a growing number of quantum chemistry-based dynamics simulations on metal-catalyzed reactions—[28,29,61,74−78] have revealed exceedingly complex reaction networks for Davies' Rh_2L_4-promoted C−H(C) functionalization/Cope rearrangements. These results confirm Davies et al.'s original proposal of a flat potential energy surface with a PTSB and showcase the even greater complexity of the reaction network tied to this surface and the dynamical behavior of the molecules faced with traversing it. Of particular note, the importance of s-*cis*/s-*trans* ratios in preparing trajectories to launch was revealed, as was the importance of flat regions of the post-TS energy surface, which allow for entropic intermediates. The "dynamic mismatching" concept was introduced as a twist on Carpenter's dynamic matching concept, and a tentative model of the origins of increased selectivity with DOSP ligands was put forth. The general importance of post-transition state dynamics for controlling selectivity in Rh_2L_4-promoted reactions now seems quite clear.

ASSOCIATED CONTENT

Supporting Information

The Supporting Information is available free of charge at https://pubs.acs.org/doi/10.1021/jacs.4c00382.

https://doi.org/10.1021/jacs.4c00382
J. Am. Chem. Soc. 2024, 146, 7039−7051

Additional computational results and discussion, including information on other conformations of CH activation TSs IRC plots, and uphill dynamics simulations (PDF)
Movie of a key trajectory (MP4)
Movie of a key trajectory (MP4)
Movie of a key trajectory (MP4)

AUTHOR INFORMATION

Corresponding Author

Dean J. Tantillo − *Department of Chemistry, University of California, Davis, Davis, California 95616, United States;* orcid.org/0000-0002-2992-8844; Email: djtantillo@ucdavis.edu

Author

Wentao Guo − *Department of Chemistry, University of California, Davis, Davis, California 95616, United States;* orcid.org/0000-0001-8058-8323

Complete contact information is available at: https://pubs.acs.org/10.1021/jacs.4c00382

Notes

The authors declare no competing financial interest.

ACKNOWLEDGMENTS

We gratefully acknowledge support, both financial and computational (via the ACCESS program), from the National Science Foundation (CHE-2154083 and CHE-2247836).

REFERENCES

(1) Frenking, G.; Solà, M.; Vyboishchikov, S. F. Chemical Bonding in Transition Metal Carbene Complexes. *J. Organomet. Chem.* **2005**, *690* (24−25), 6178−6204.
(2) Doyle, M. P. Catalytic Methods for Metal Carbene Transformations. *Chem. Rev.* **1986**, *86* (5), 919−939.
(3) Cardin, D. J.; Cetinkaya, B.; Lappert, M. F. Transition Metal-Carbene Complexes. *Chem. Rev.* **1972**, *72*, 545−574.
(4) Hansen, J.; Davies, H. M. L. High Symmetry Dirhodium(II) Paddlewheel Complexes as Chiral Catalysts. *Coord. Chem. Rev.* **2008**, *252* (5−7), 545−555.
(5) Wu, R.; Zhu, D.; Zhu, S. Dirhodium: Carbene Transformations and Beyond. *Org. Chem. Front.* **2023**, *10* (11), 2849−2878.
(6) Adly, F. G. On the Structure of Chiral Dirhodium(II) Carboxylate Catalysts: Stereoselectivity Relevance and Insights for Improved Performance of Viable Whole-Cell Baeyer-Villiger Monoxygenase by Immobilization. *Catalysts* **2017**, *7* (11), 347.
(7) Taber, D. F.; Petty, E. H. General Route to Highly Functionalized Cyclopentane Derivatives by Intramolecular C-H Insertion. *J. Org. Chem.* **1982**, *47* (24), 4808−4809.
(8) Xiang, Y.; Wang, C.; Ding, Q.; Peng, Y. Diazo Compounds: Versatile Synthons for the Synthesis of Nitrogen Heterocycles via Transition Metal-Catalyzed Cascade C−H Activation/Carbene Insertion/Annulation Reactions. *Adv. Synth. Catal.* **2019**, *361* (5), 919−944.
(9) Davies, H. M. L.; Liao, K. Dirhodium Tetracarboxylates as Catalysts for Selective Intermolecular C−H Functionalization. *Nat. Rev. Chem.* **2019**, *3* (6), 347−360.
(10) Davies, H. M. L.; Panaro, S. A. Effect of Rhodium Carbenoid Structure on Cyclopropanation Chemoselectivity. *Tetrahedron* **2000**, *56* (28), 4871−4880.
(11) Chuprakov, S.; Kwok, S. W.; Zhang, L.; Lercher, L.; Fokin, V. V. Rhodium-Catalyzed Enantioselective Cyclopropanation of Olefins with N-Sulfonyl 1,2,3-Triazoles. *J. Am. Chem. Soc.* **2009**, *131* (50), 18034−18035.
(12) Gurmessa, G. T.; Singh, G. S. Recent Progress in Insertion and Cyclopropanation Reactions of Metal Carbenoids from α-Diazocarbonyl Compounds. *Res. Chem. Intermed.* **2017**, *43* (11), 6447−6504.
(13) Qi, X.; Lan, Y. Recent Advances in Theoretical Studies on Transition-Metal-Catalyzed Carbene Transformations. *Acc. Chem. Res.* **2021**, *54* (14), 2905−2915.
(14) Lledós, A. Computational Organometallic Catalysis: Where We Are, Where We Are Going. *Eur. J. Inorg. Chem.* **2021**, *2021* (26), 2547−2555.
(15) Taber, D. F.; You, K. K.; Rheingold, A. L. Predicting the Diastereoselectivity of Rh-Mediated Intramolecular C-H Insertion. *J. Am. Chem. Soc.* **1996**, *118* (3), 547−556.
(16) Lee, M.; Ren, Z.; Musaev, D. G.; Davies, H. M. L. Rhodium-Stabilized Diarylcarbenes Behaving as Donor/Acceptor Carbene. *ACS Catal.* **2020**, *10* (11), 6240−6247.
(17) Lu, G.; Fang, C.; Xu, T.; Dong, G.; Liu, P. Computational Study of Rh-Catalyzed Carboacylation of Olefins: Ligand-Promoted Rhodacycle Isomerization Enables Regioselective C-C Bond Functionalization of Benzocyclobutenones. *J. Am. Chem. Soc.* **2015**, *137* (25), 8274−8283.
(18) Cammarota, R. C.; Liu, W.; Bacsa, J.; Davies, H. M. L.; Sigman, M. S. Mechanistically Guided Workflow for Relating Complex Reactive Site Topologies to Catalyst Performance in C-H Functionalization Reactions. *J. Am. Chem. Soc.* **2022**, *144* (4), 1881−1898.
(19) Nakamura, E.; Yoshikai, N.; Yamanaka, M. Mechanism of C-H Bond Activation/C-C Bond Formation Reaction between Diazo Compound and Alkane Catalyzed by Dirhodium Tetracarboxylate. *J. Am. Chem. Soc.* **2002**, *124* (24), 7181−7192.
(20) Ren, Z.; Musaev, D. G.; Davies, H. M. L. Key Selectivity Controlling Elements in Rhodium-Catalyzed C-H Functionalization with Donor/Acceptor Carbenes. *ACS Catal.* **2022**, *12*, 13446−13456.
(21) Quapp, W.; Hirsch, M.; Heidrich, D. Bifurcation of Reaction Pathways: The Set of Valley Ridge Inflection Points of a Simple Three-Dimensional Potential Energy Surface. *Theor. Chem. Acc.* **1998**, *100* (5−6), 285−299.
(22) Thomas, J. B.; Waas, J. R.; Harmata, M.; Singleton, D. A. Control Elements in Dynamically Determined Selectivity on a Bifurcating Surface. *J. Am. Chem. Soc.* **2008**, *130*, 14544−14555.
(23) Quapp, W.; Hirsch, M.; Heidrich, D. An Approach to Reaction Path Branching Using Valley-Ridge Inflection Points of Potential-Energy Surfaces. *Theor. Chem. Acc.* **2004**, *112* (1), 40−51.
(24) Ess, D. H.; Wheeler, S. E.; Iafe, R. G.; Xu, L.; Çelebi-Ölçüm, N.; Houk, K. N. Bifurcations on Potential Energy Surfaces of Organic Reactions. *Angew. Chemie - Int. Ed.* **2008**, *47* (40), 7592−7601.
(25) Carpenter, B. K. Energy Disposition in Reactive Intermediates. *Chem. Rev.* **2013**, *113* (9), 7265−7286.
(26) Tantillo, D. J. Dynamic Effects on Organic Reactivity—Pathways to (and from) Discomfort. *J. Phys. Org. Chem.* **2021**, *34*, No. e4202.
(27) Zhang, H.; Novak, A. J. E.; Jamieson, C. S.; Xue, X. S.; Chen, S.; Trauner, D.; Houk, K. N. Computational Exploration of the Mechanism of Critical Steps in the Biomimetic Synthesis of Preuisolactone A, and Discovery of New Ambimodal (5 + 2)/(4 + 2) Cycloadditions. *J. Am. Chem. Soc.* **2021**, *143* (17), 6601−6608.
(28) Hare, S. R.; Tantillo, D. J. Cryptic Post-Transition State Bifurcations That Reduce the Efficiency of Lactone-Forming Rh-Carbenoid C-H Insertions. *Chem. Sci.* **2017**, *8* (2), 1442−1449.
(29) Guo, W.; Hare, S. R.; Chen, S. S.; Saunders, C. M.; Tantillo, D. J. C-H Insertion in Dirhodium Tetracarboxylate-Catalyzed Reactions Despite Dynamical Tendencies toward Fragmentation: Implications for Reaction Efficiency and Catalyst Design. *J. Am. Chem. Soc.* **2022**, *144* (37), 17219−17231.
(30) Davies, H. M. L.; Lian, Y. The Combined C-H Functionalization/Cope Rearrangement: Discovery and Applications in Organic Synthesis. *Acc. Chem. Res.* **2012**, *45* (6), 923−935.
(31) Hansen, J. H.; Gregg, T. M.; Ovalles, S. R.; Lian, Y.; Autschbach, J.; Davies, H. M. L. On the Mechanism and Selectivity of

the Combined C-H Activation/Cope Rearrangement. *J. Am. Chem. Soc.* **2011**, *133* (13), 5076−5085.
(32) Davies, H. M. L.; Stafford, D. G.; Hansen, T. Catalytic Asymmetric Synthesis of Diarylacetates and 4,4-Diarylbutanoates. A Formal Asymmetric Synthesis of (+)-Sertraline. *Org. Lett.* **1998**, *1* (2), 233−236.
(33) Thompson, J. L.; Davies, H. M. L. Enhancement of Cyclopropanation Chemistry in the Silver-Catalyzed Reactions of Aryldiazoacetates. *J. Am. Chem. Soc.* **2007**, *129* (19), 6090−6091.
(34) Lourderaj, U.; Park, K.; Hase, W. L. Classical Trajectory Simulations of Post-Transition State Dynamics. *Int. Rev. Phys. Chem.* **2008**, *27* (3), 361−403.
(35) Davies, H. M. L.; Stafford, D. G.; Doan, B. D.; Houser, J. H. Tandem Asymmetric Cyclopropanation/Cope Rearrangement. A Highly Diastereoselective and Enantioselective Method for the Construction of 1,4-Cycloheptadienes. *J. Am. Chem. Soc.* **1998**, *120* (14), 3326−3331.
(36) Marichev, K. O.; Zheng, H.; Doyle, M. P.Metal Carbene Cycloaddition Reactions. In *Transition Metal-Catalyzed Carbene Transformations*Wang, Jianbo, Che, Chi-Ming, Doyle, Michael P. Eds.; WILEY-VCH, 2022; pp 139−168.
(37) Frisch, M. J.; Trucks, G. W.; Schlegel, H. B.; Scuseria, G. E.; Robb, M. A.; Cheeseman, J. R.; Scalmani, G.; Barone, V.; Petersson, G. A.; Nakatsuji, H.; Li, X.; Caricato, M.; Marenich, A. V.; Bloino, J.; Janesko, B. G.; Gomperts, R.; Mennucci, B.; Hratchian, H. P., *Gaussian 16, Revision C.01* Gaussian, Inc. 2016.
(38) Becke, A. D. Density-Functional Exchange-Energy Approximation with Correct Asymptotic Behavior. *J. Chem. Phys.* **1936**, *4* (4), 276−282.
(39) Sperger, T.; Sanhueza, I. A.; Kalvet, I.; Schoenebeck, F. Computational Studies of Synthetically Relevant Homogeneous Organometallic Catalysis Involving Ni, Pd, Ir, and Rh: An Overview of Commonly Employed DFT Methods and Mechanistic Insights. *Chem. Rev.* **2015**, *115* (17), 9532−9586.
(40) Grimme, S. Density Functional Theory with London Dispersion Corrections. *Wiley Interdiscip. Rev. Comput. Mol. Sci.* **2011**, *1* (2), 211−228.
(41) Ditchfield, R.; Hehre, W. J.; Pople, J. A. Self-Consistent Molecular-Orbital Methods. IX. An Extended Gaussian-Type Basis for Molecular-Orbital Studies of Organic Molecules. *J. Chem. Phys.* **1971**, *54* (2), 720−723.
(42) Hay, P. J.; Wadt, W. R. Ab Initio Effective Core Potentials for Molecular Calculations. Potentials for K to Au Including the Outermost Core Orbitals. *J. Chem. Phys.* **1985**, *82* (1), 299−310.
(43) Zhao, Y.; Truhlar, D. G. The M06 Suite of Density Functionals for Main Group Thermochemistry, Thermochemical Kinetics, Noncovalent Interactions, Excited States, and Transition Elements: Two New Functionals and Systematic Testing of Four M06-Class Functionals and 12 Other Functionals. *Theor. Chem. Acc.* **2008**, *120* (1−3), 215−241.
(44) Curtiss, L. A.; McGrath, M. P.; Blaudeau, J. P.; Davis, N. E.; Binning, R. C.; Radom, L. Extension of Gaussian-2 Theory to Molecules Containing Third-Row Atoms Ga-Kr. *J. Chem. Phys.* **1995**, *103* (14), 6104−6113.
(45) Kumar, M.; Chaudhari, R. V.; Subramaniam, B.; Jackson, T. A. Ligand Effects on the Regioselectivity of Rhodium-Catalyzed Hydroformylation: Density Functional Calculations Illuminate the Role of Long-Range Noncovalent Interactions. *Organometallics* **2014**, *33* (16), 4183−4191.
(46) Cossi, M.; Barone, V.; Cammi, R.; Tomasi, J. Ab Initio Study of Solvated Molecules: A New Implementation of the Polarizable Continuum Model. *Chem. Phys. Lett.* **1996**, *255* (4−6), 327−335.
(47) Miertuš, S.; Scrocco, E.; Tomasi, J. Electrostatic Interaction of a Solute with a Continuum. A Direct Utilizaion of Ab Initio Molecular Potentials for the Prevision of Solvent Effects. *Chem. Phys.* **1981**, *55* (1), 117−129.
(48) Fukui, K. The Path of Chemical Reactions — The IRC Approach. *Acc. Chem. Res.* **1981**, *14* (12), 363−368.
(49) Page, M.; McIver, J. W. On Evaluating the Reaction Path Hamiltonian. *J. Chem. Phys.* **1988**, *88* (2), 922−935.
(50) Page, M.; Doubleday, C.; McIver, J. W. Following Steepest Descent Reaction Paths. The Use of Higher Energy Derivatives with Ab Initio Electronic Structure Methods. *J. Chem. Phys.* **1990**, *93* (8), 5634−5642.
(51) Álvarez-Moreno, M.; De Graaf, C.; López, N.; Maseras, F.; Poblet, J. M.; Bo, C. Managing the Computational Chemistry Big Data Problem: The IoChem-BD Platform. *J. Chem. Inf. Model.* **2015**, *55* (1), 95−103.
(52) Ussing, B. R.; Hang, C.; Singleton, D. A. Dynamic Effects on the Periselectivity, Rate, Isotope Effects, and Mechanism of Cycloadditions of Ketenes with Cyclopentadiene. *J. Am. Chem. Soc.* **2006**, *128* (23), 7594−7607.
(53) Bao, J. L.; Truhlar, D. G. Variational Transition State Theory: Theoretical Framework and Recent Developments. *Chem. Soc. Rev.* **2017**, *46* (24), 7548−7596.
(54) Zheng, J.; Bao, J. L.; Meana-Pañeda, R.; Zhang, S.; Lynch, B. J.; Corchado, J. C.; Chuang, Y.-Y.; Fast, P. L.; Hu, W.-P.; Liu, Y.-P.; Lynch, G. C.; Nguyen, K. A.; Jackels, C. F.; Fernandez Ramos, A.; Ellingson, B. A.; Melissas, V. S.; Villà, J.; Rossi, I.; Coitiño, E. L.; Pu, J.; Albu, T. V.; Ratkiewicz, A.; Steckler, R.; Garrett, B. C.; Isaacson, A. D.; Truhlar, D. G. *Polyrate-version 2017-C*; University of Minnesota: Minneapolis, 2017.
(55) Zheng, J.; Bao, J. L.; Zhang, S.; Corchado, J. C.; Meana-Pañeda, R.; Chuang, Y.-Y.; Coitiño, E. L.; Ellingson, B. A.; Truhlar, D. G. *Gaussrate 17*; University of Minnesota: Minneapolis, 2017.
(56) Feng, Z.; Tantillo, D. J. Dynamic Effects on Migratory Aptitudes in Carbocation Reactions. *J. Am. Chem. Soc.* **2021**, *143* (2), 1088−1097.
(57) Nieves-Quinones, Y.; Singleton, D. A. Dynamics and the Regiochemistry of Nitration of Toluene. *J. Am. Chem. Soc.* **2016**, *138* (46), 15167−15176.
(58) Tremblay, M. T.; Yang, Z. J. The Effect of Zero-Point Energy in Simulating Organic Reactions with Post-Transition State Bifurcation. *J. Phys. Org. Chem.* **2022**, *35* (11), 1−7.
(59) Legault, C. Y. *CYLview*. Univ. Sherbrooke 2009.
(60) Yang, Z.; Jamieson, C. S.; Xue, X. S.; Garcia-Borràs, M.; Benton, T.; Dong, X.; Liu, F.; Houk, K. N. Mechanisms and Dynamics of Reactions Involving Entropic Intermediates. *Trends Chem.* **2019**, *1* (1), 22−34.
(61) Joy, J.; Ess, D. H. Direct Dynamics Trajectories Demonstrate Dynamic Matching and Nonstatistical Radical Pair Intermediates during Fe-Oxo-Mediated C-H Functionalization Reactions. *J. Am. Chem. Soc.* **2023**, *145*, 7628−7637.
(62) Gonzalez-James, O. M.; Kwan, E. E.; Singleton, D. A. Entropic Intermediates and Hidden Rate-Limiting Steps in Seemingly Concerted Cycloadditions. Observation, Prediction, and Origin of an Isotope Effect on Recrossing. *J. Am. Chem. Soc.* **2012**, *134* (4), 1914−1917.
(63) Peterson, T. H.; Carpenter, B. K. Estimation of Dynamic Effects on Product Ratios by Vectorial Decomposition of a Reaction Coordinate. Application to Thermal Nitrogen Loss from Bicyclic Azo Compounds. *J. Am. Chem. Soc.* **1992**, *114* (2), 766−767.
(64) Lu, T.; Chen, F. Multiwfn: A Multifunctional Wavefunction Analyzer. *J. Comput. Chem.* **2012**, *33* (5), 580−592.
(65) Humphrey, W.; Dalke, A.; Schulten, K. VMD: Visual Molecular Dynamics. *J. Mol. Graph.* **1996**, *14* (1), 33−38.
(66) Carpenter, B. K. Dynamic Matching: The Cause of Inversion of Configuration in the [1, 3] Sigmatropic Migration? *J. Am. Chem. Soc.* **1995**, *117* (23), 6336−6344.
(67) Törk, L.; Jiménez-Osés, G.; Doubleday, C.; Liu, F.; Houk, K. N. Molecular Dynamics of the Diels-Alder Reactions of Tetrazines with Alkenes and N_2 Extrusions from Adducts. *J. Am. Chem. Soc.* **2015**, *137* (14), 4749−4758.
(68) Chen, Z.; Nieves-Quinones, Y.; Waas, J. R.; Singleton, D. A. Isotope Effects, Dynamic Matching, and Solvent Dynamics in a Wittig Reaction. Betaines as Bypassed Intermediates. *J. Am. Chem. Soc.* **2014**, *136* (38), 13122−13125.

https://doi.org/10.1021/jacs.4c00382
J. Am. Chem. Soc. 2024, 146, 7039−7051

(69) Wang, Z.; Hirschi, J. S.; Singleton, D. A. Recrossing and Dynamic Matching Effects on Selectivity in a Diels-Alder Reaction. *Angew. Chemie - Int. Ed.* **2009**, *48* (48), 9156−9159.
(70) Davies, H. M. L.; Morton, D. Guiding Principles for Site Selective and Stereoselective Intermolecular C−H Functionalization by Donor/Acceptor Rhodium Carbenes. *Chem. Soc. Rev.* **2011**, *40* (4), 1857−1869.
(71) Briones, J. F.; Hansen, J.; Hardcastle, K. I.; Autschbach, J.; Davies, H. M. L. Highly Enantioselective Rh_2(*s*-DOSP)$_4$-Catalyzed Cyclopropenation of Alkynes with Styryldiazoacetates. *J. Am. Chem. Soc.* **2010**, *132* (48), 17211−17215.
(72) Werlé, C.; Goddard, R.; Philipps, P.; Farès, C.; Fürstner, A. Stabilization of a Chiral Dirhodium Carbene by Encapsulation and a Discussion of the Stereochemical Implications. *Angew. Chemie - Int. Ed.* **2016**, *55* (36), 10760−10765.
(73) Grimme, S. Exploration of Chemical Compound, Conformer, and Reaction Space with Meta-Dynamics Simulations Based on Tight-Binding Quantum Chemical Calculations. *J. Chem. Theory Comput.* **2019**, *15* (5), 2847−2862.
(74) Feng, Q.; Wu, H.; Li, X.; Song, L.; Chung, L. W.; Wu, Y.-D.; Sun, J. Ru-Catalyzed Geminal Hydroboration of Silyl Alkynes via a New Gem-Addition Mechanism. *J. Am. Chem. Soc.* **2020**, *142* (32), 13867−13877.
(75) Yang, Y.; Zhang, X.; Zhong, L.-P.; Lan, J.; Li, X.; Li, C.-C.; Chung, L. W. Unusual KIE and Dynamics Effects in the Fe-Catalyzed Hetero-Diels-Alder Reaction of Unactivated Aldehydes and Dienes. *Nat. Commun.* **2020**, *11* (1), 1850.
(76) Teynor, M. S.; Scott, W.; Ess, D. H. Catalysis with a Skip: Dynamically Coupled Addition, Proton Transfer, and Elimination during Au- and Pd-Catalyzed Diol Cyclizations. *ACS Catal.* **2021**, *11* (16), 10179−10189.
(77) Joy, J.; Schaefer, A. J.; Teynor, M. S.; Ess, D. H. Dynamical Origin of Rebound versus Dissociation Selectivity during Fe-Oxo-Mediated C-H Functionalization Reactions. *J. Am. Chem. Soc.* **2024**, *146* (4), 2452−2464.
(78) Ziegler, T.; Autschbach, J. Theoretical Methods of Potential Use for Studies of Inorganic Reaction Mechanisms. *J. Chem. Rev.* **2005**, *105* (6), 2695−2722.

https://doi.org/10.1021/jacs.4c00382
J. Am. Chem. Soc. 2024, 146, 7039−7051